ACS OMEGA

http://pubs.acs.org/journal/acsodf

Article

Catalytic Oxidation of Toluene into Benzaldehyde and Benzyl Alcohol Using Molybdenum-Incorporated Manganese Oxide Nanomaterials

Hamza Shoukat, Ataf Ali Altaf,* Muhammad Hamayun, Shaheed Ullah, Samia Kausar, Muhammad Hamza, Shabbir Muhammad, Amin Badshah, Nasir Rasool, and Muhammad Imran

Cite This: *ACS Omega* 2021, 6, 19606−19615

Read Online

ACCESS | Metrics & More | Article Recommendations

ABSTRACT: Oxidation of toluene (an organic pollutant), into useful chemical products, is of great interest nowadays. However, efficient conversion of toluene under mild and sustainable conditions is a thought-provoking task. Here, we report $MnMoO_4$ nanomaterials (**CH1**−**CH2**), synthesized through a very facile solvothermal approach. Catalytic efficiencies of $MnMoO_4$ nanomaterials were evaluated by direct oxidation of toluene via C−H activation. Toluene was converted into benzaldehyde and benzyl alcohol in the presence of H_2O_2 as an oxidant at 80 °C. The reaction parameters, that is, catalyst dose, time, and toluene concentration, were varied to obtain the optimal conditions for the oxidation process. The 40.62% maximum toluene conversion rate was obtained after 18 h of oxidation activity with 0.06 g of catalyst **CH1**. A maximum of 78% benzaldehyde selectivity was obtained with 0.06 g of catalyst **CH1** after 18 h of toluene oxidation activity. Also, 62.33% benzyl alcohol selectivity was achieved using 0.1 g of catalyst **CH1** after 1 h of activity. Several catalytic cycles were run with **CH1** to evaluate catalyst reusability. Potential % toluene conversion was obtained for up to six cycles and their turnover frequencies were found to be 1.94−1.01 s^{-1}. FTIR spectra of catalyst **CH1** before and after recovery indicate no significant change. The good conversion rate of toluene and efficient selectivity toward benzaldehyde and benzyl alcohol indicates the robustness and high potential of these catalysts to oxidize toluene under a milder, greener, and hazardous chlorine-free environment.

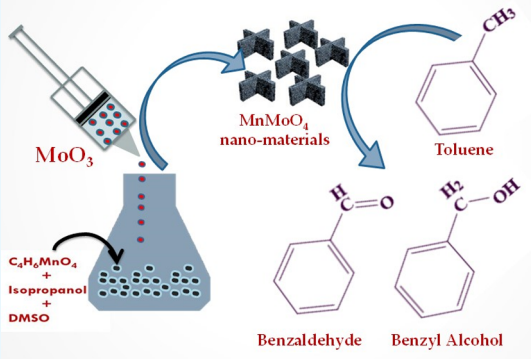

1. INTRODUCTION

Benzaldehyde and benzyl alcohol are the simple members of aromatic hydrocarbons[1] and are considered as prime starting materials in various industries such as pharmaceutical,[2] perfumery, soaps, chemicals, and plastic industry.[3] The safer industrial production of these aldehydes and alcohols is still a challenging task; this is mainly done through chlorination of toluene and subsequent hydrolysis.[4] Toluene is a cheaper industrial chemical, less toxic, easy to handle, and used for the production of chemicals such as benzaldehyde and benzyl alcohol. However, the major drawback of this process is that it requires very punitive reaction conditions and produces toxic waste in the form of chlorinated species which are harmful to the environment and cause equipment corrosion. Besides, this process needs expensive separation protocols and also is less selective toward products.[5] Oxidation of toluene has been a challenging task for researchers with mild and environmentally friendly conditions.[6] Although several catalysts have been synthesized for this purpose in the past few decades, new catalytic routes have been investigated for this purpose which have mainly involved the homogeneous catalysts such as metal complexes of copper, manganese, iron (III)-containing porphyrins, Schiff bases, tetraazaanulenes, chlorins, and triazacyclononane ligands.[7] However, while homogeneous catalysts speed up the reactions, they also have limitations such as cost, difficulty in the synthesis of ligands along with poor selectivity, and lesser recyclability, which cut them off from practical and industrial usage.[8] Moreover, large-scale production and removal of a minute quantity of catalysts have been challenging tasks that lead to the failure of homogeneous catalysts for the oxidation of toluene at the industrial level. To reduce such logjams, researchers have been indulged in efforts to synthesize heterogeneous catalysts for oxidation of toluene into other industrial products. Heterogeneous catalysts have

Received: April 23, 2021
Accepted: July 6, 2021
Published: July 20, 2021

ACS Publications

© 2021 The Authors. Published by American Chemical Society

various unique characteristics which make them superior to homogeneous catalysts, such as easy recovery/separation of the catalyst,[9] straightforward synthesis process, higher recyclability, and increase in selectivity toward yields.[10] Besides, these catalysts also provide a green approach toward synthetic chemistry by limiting the consumption of toxic and hazardous chemicals in synthetic routes.[11] For instance, noble metals such as silver,[12] gold,[13] platinum,[14] palladium,[10] and ruthenium[15] have been used in the catalysis of various organic reactions such as selective oxidation of aromatic alkanes, alcohols, and nitriles along with the utilization of milder oxidants such as air, oxygen, and hydrogen peroxide.[16] These heterogeneous catalysts do C−H activation and oxidized toluene into various products as mentioned above; however, many of such catalysts do not involve a greener route and pollute the ecosystem. Another approach to address this issue has been exploited, where metal oxides supported over noble metals used for the oxidation of toluene, such as Ag/WO_3[16] and $Ag-Pd/TiO_2$,[17] have shown greater efficiency in toluene oxidation via C−H activation. Besides, bimetallic manganese-based oxides have been used for the degradation of toluene.[18,19] However, to find a reliable and efficient method for the oxidation of toluene is still of great demand.

$MnMoO_4$, a mixed metal oxide of manganese and molybdenum also called manganese molybdate, has recently been reported in nanotechnology in various applications, such as supercapacitors,[20] electrode materials in lithium-ion batteries,[21] energy-storage devices,[22] and as photocatalysts.[23,24] However, manganese molybdate has not been used in the oxidation of toluene to the best of the author's knowledge.

Here, we report a single-step, facile, and cost-effective hydrothermal method for the synthesis of $MnMoO_4$ for the oxidation of toluene into benzaldehyde and benzyl alcohol (Figure 1). The hydrothermal procedure is profitable and the simplest procedure for the large-scale synthesis of water-insoluble metal oxides with high purity and controllable morphology using water-soluble metal precursors at high pressure and moderate temperature. All the synthetic and catalytic routes implied in this regard are safer, eco-friendly, less toxic, and cheaper. Therefore, $MnMoO_4$ was used as heterogeneous catalysts for the thermal oxidation of toluene in the liquid phase via C−H activation and has shown notable activity in this regard. Hope this work will open new ways in catalysis and material preparation.

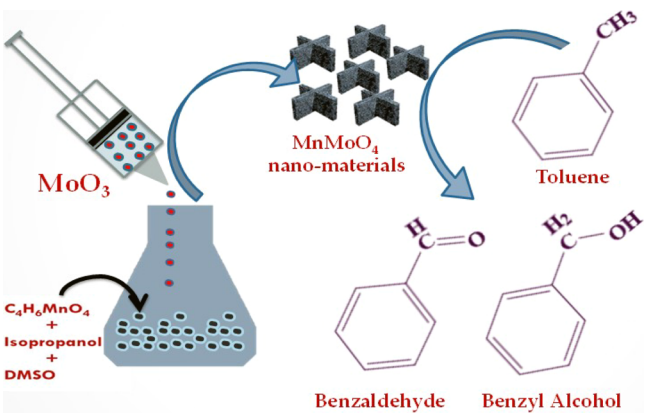

Figure 1. Schematics of $MnMoO_4$ nanomaterial preparation and toluene oxidation to benzaldehyde and benzyl alcohol.

2. RESULTS AND DISCUSSION

2.1. Characterization of the Synthesized Nanomaterials. *2.1.1. PXRD Analysis.* The phase composition and particle size of the synthesized materials (**CH1**−**CH2**) were analyzed by powder X-ray diffraction (PXRD) and the evaluated data are enlisted in Table 1. The PXRD patterns of the synthesized catalysts **CH1** and **CH2** are presented in Figure 2. Specific hkl values were evaluated for diffraction peaks against the corresponding 2θ values. These hkl values were matched with the standard PXRD patterns of $MnMoO_4$ (JCPDS card no. 27-1280). PXRD analysis indicated that the crystal structure of the synthesized materials **CH1** and **CH2** is triclinic and characteristic peaks are indexed to lattice planes 001, 111, 002, 021, 301, 141, and 224 concise to the standard pattern.[22]

The crystallite sizes of all the samples have been calculated using the Debye−Scherer eq 1.[25]

$$D = \frac{k\lambda}{\beta \cos \theta} \tag{1}$$

where D is the average crystallite size (nm), k is a constant having a value of 0.9, λ is the wavelength of the source of Cu-Kα, having a value of 0.15406 nm, β is the full width of the peak at half-maxima (fwhm), and θ is the angle (radian) which can be obtained from PXRD patterns of the as-prepared materials. The average crystallite size for **CH1** and **CH2** was calculated as 52.7 and 52.6 nm, respectively.

The volume (V) of crystals[26] was calculated using relation ($V = D^3$) and listed in Table 1. Dislocation density denoted by (δ) is related to defects in the crystalline system and is defined as the length of dislocation lines per unit volume of the crystal and has been calculated from equation ($\delta = 1/D^2$) and described in Table 1.[27] Microstrain (ε)-induced broadening in powder due to crystal imperfection and distortion has also been calculated using eq 2.

$$\varepsilon = \frac{\beta}{4 \tan \theta} \tag{2}$$

and is reported in Table 1 for all samples synthesized; positive values of ε represent tensile strain, while negative relates to compression strain in crystals.[28]

2.1.2. SEM and EDX Analysis. Surface morphological characteristics of the synthesized materials **CH1** and **CH2** were evaluated by scanning electron microscopy (SEM) analysis for which SEM micrographs are presented in Figure 3. SEM images of **CH1** and **CH2** have shown broad surfaces with squares and cross-type shapes.

The elemental analysis of the synthesized materials was carried out by energy-dispersive X-ray (EDX) analysis. The EDX images obtained are presented in Figure 3. The EDX image of **CH1** and **CH2** exhibited various peaks for manganese, molybdenum, and oxygen with a varying intensity which confirmed the presence of all these elements in samples. The individual weight percent of elements for **CH1** was calculated as Mn(37.03), Mo(35.14), and O(27.82), whereas for **CH2**, it was calculated as Mn(43.54), Mo(30.21), and O(26.24).

2.1.3. UV−Vis Spectroscopic and PL Analysis. UV−vis, photoluminescence (PL), and FTIR analyses are carried out to evaluate the optical properties of the synthesized materials. The absorption spectra are presented in Figure 4. The direct and indirect band gap energy values of **CH1** and **CH2** are

https://doi.org/10.1021/acsomega.1c02163
ACS Omega 2021, 6, 19606−19615

Table 1. Synthesis Conditions and PXRD and SEM/EDX Parameters Calculated for the Synthesized Nanomaterials (CH1−CH2)

property	CH1	CH2
synthesis conditions	3.5 g of Mn-acetate, 30 mL of isopropanol, 10 mL of DMSO, and 2.2 g of MoO_3	3.5 g Mn-acetate, 30 mL of isopropanol, 10 mL of DMSO, 1.73 g MoO_3
crystallite Size D (nm)	52.7	52.6
volume $V = D^3$	144,419.1	145,531.6
dislocation density ×10−3 (δ) (nm−2)	3.6×10^{-4}	3.8×10^{-4}
microstrain (ε)	0.0160	0.0233
found percentage composition of each element (By EDX)	Mn(37.03), Mo(35.14), and O(27.82)	Mn(43.54), Mo(30.21) and O(26.24)
structural appearance (By SEM)	square and cross type	square and cross type

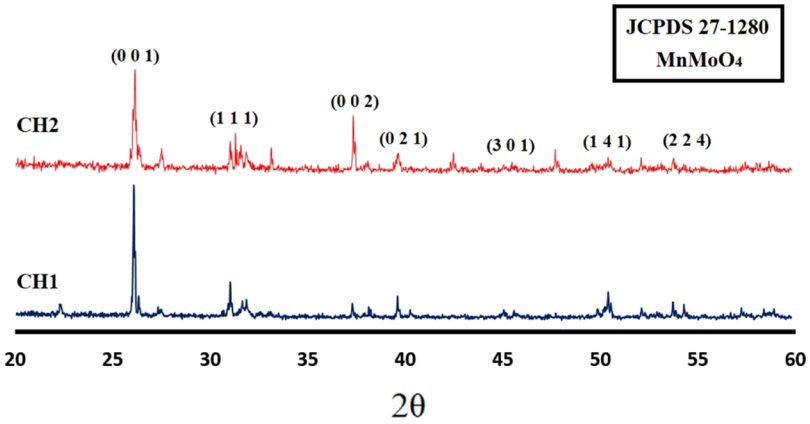

Figure 2. PXRD patterns of the synthesized materials (**CH1−CH2**) [powder patterns are matched with the standard pattern of $MnMoO_4$ (JCPD no. 27-1280)].

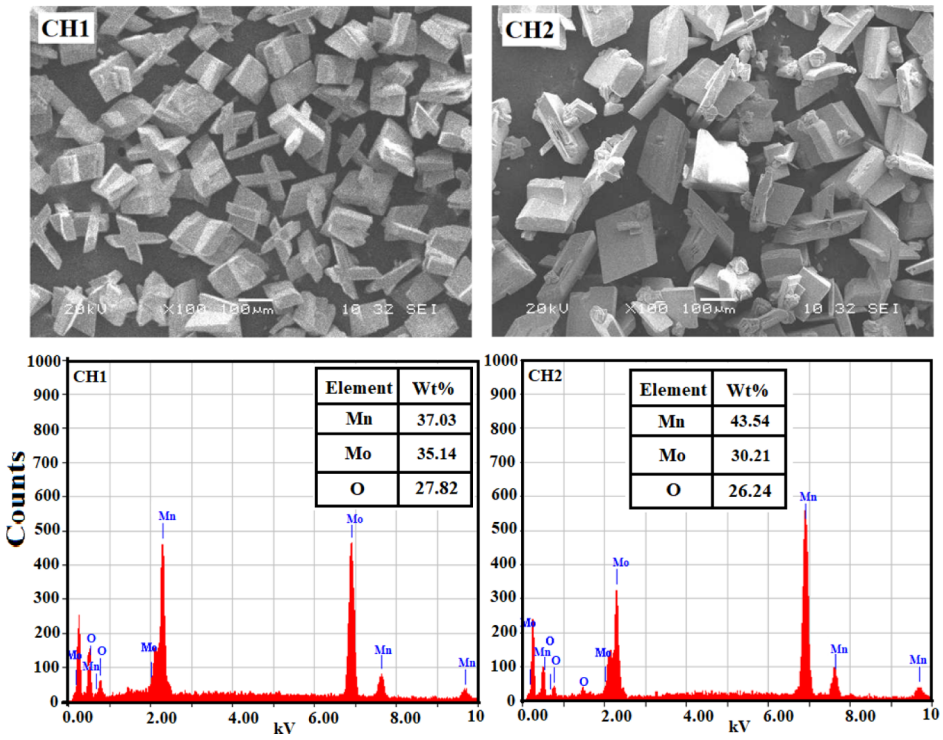

Figure 3. SEM and EDX Images of the Synthesized Materials **CH1** and **CH2**.

calculated from absorption spectra using the Tauc plot equation (eqs 3a3a and 3b3b).[29]

$$\text{Direct bang gap}(\alpha h\nu)^2 = A(h\nu - E_g) \tag{3a}$$

$$\text{Indirect bang gap}(\alpha h\nu)^{1/2} = A(h\nu - E_g) \tag{3b}$$

where $h\nu$ is the incident photon energy, "α" is the absorption coefficient, "A" is the proportionality constant, and "E_g" is the

https://doi.org/10.1021/acsomega.1c02163
ACS Omega 2021, 6, 19606−19615

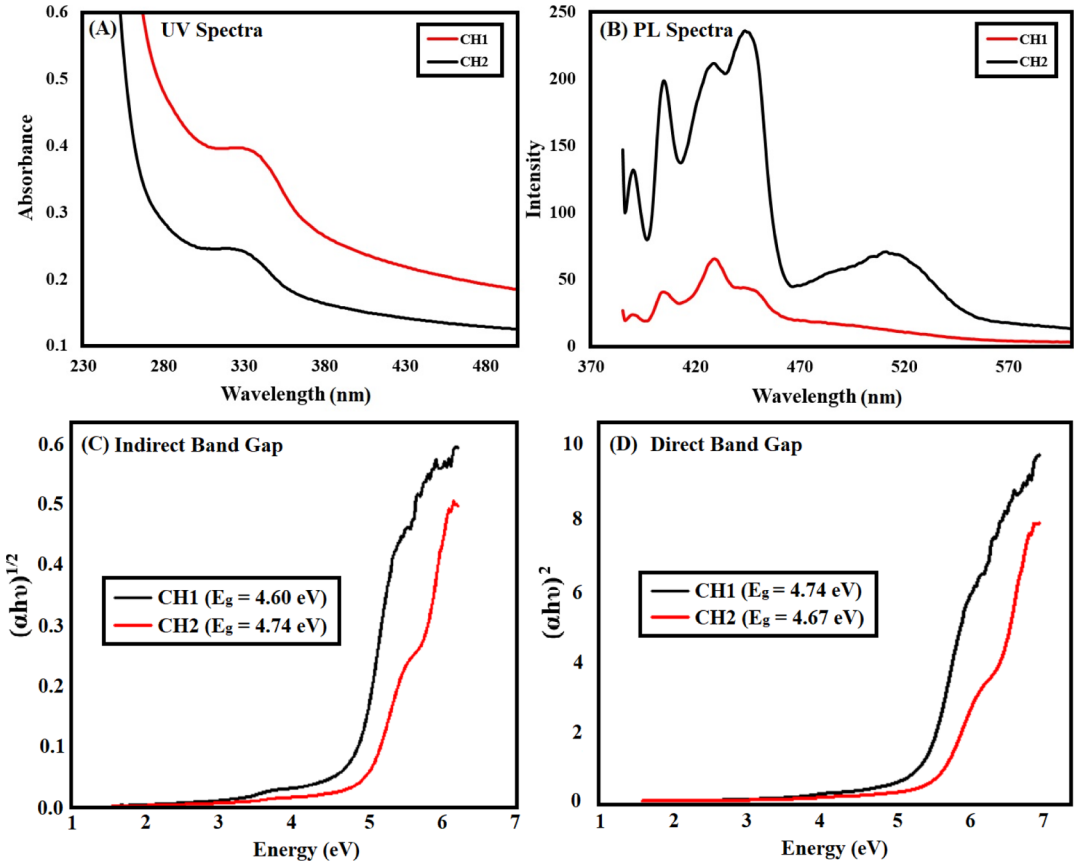

Figure 4. UV and PL spectra and direct and indirect band gap of nanomaterials (**CH1**−**CH2**).

band gap energy. Direct energy band gaps for **CH1** and **CH2** were calculated as 4.74 and 4.67 eV and indirect band gaps as 4.60 and 4.74 eV, respectively, indicating the ability of the synthesized materials to absorb light in the UV-to-visible region, hence will readily exhibit the catalytic properties.[30]

PL studies were carried out to evaluate the trapping efficiency of charge carriers, transfer, and migration to apprehend the fate of electron−hole pairs in the material.[24] The PL spectra of the synthesized nanomaterials **CH1** and **CH2** are represented in Figure 4B. The PL spectra are differentiated into two regions; the first region is called the band edge emission region (385−400 nm). This region of the emission spectrum results from the conduction band electrons and valence band holes' recombination.[23] The second region (400−470 nm) shows that the synthesized material can be a good source to absorb UV light and emit visible light, hence a good charge carrier or migrant material and could also be used as catalysts. PL studies were carried out by giving an excitation wavelength of 375 nm, and PL spectra of all the synthesized materials were recorded. Emission peaks were observed at 390, 406, 426, and 446 nm showing increasing emission intensity for all the samples. Higher emission intensity was observed at 446 nm. It was noticed that the materials having larger band gap energy have shown peaks with increasing emission intensities.

2.1.4. Brunauer−Emmett−Teller (BET) Analysis. The specific surface area of the synthesized materials **CH1** and **CH2** was calculated by multipoint BET and the calculated parameters are enlisted in Table 2. The specific surface area for **CH1** and **CH2** was calculated as 46.32 and 42.68 m^2/g, respectively, whereas pore volume for both was in the range 0.031−0.038, indicating the mesoporous nature of the synthesized materials. Values of constant C for **CH1** and **CH2** were <100 which is usually ascribed to the ability of materials to make strong adsorbate−adsorbent interactions.

Table 2. Multipoint BET Parameters of Materials CH1 and CH2

BET Properties	samples	
	CH1	**CH2**
surface area (*S*BET) (m^2/g)	46.32	42.68
pore volume (*V*m) (cc/g)	0.038	0.031
pore width (nm)	2.573	2.178
constant *C*	20.12	18.56

2.2. Catalytic Oxidation of Toluene. Catalytic activity was performed by varying different parameters such as time, catalyst dose, and toluene concentration. Benzaldehyde and benzyl alcohol were confirmed by mass spectra obtained from GCMS analysis. Selectivity and yields of products were calculated by integration of GCMS data and are reported in Table 2. The substrate conversion, selectivity, and yield were calculated from the given equations eqs 3b−5.

$$\%\ \text{Toluene conversion} = \frac{\text{moles of toluene reacted} \times 100}{\text{initial moles of toluene}} \quad (4)$$

$$\%\ \text{Selectivity of products} = \frac{\text{moles of product formed} \times 100}{\text{moles of toluene reacted}} \quad (5)$$

https://doi.org/10.1021/acsomega.1c02163
ACS Omega 2021, 6, 19606−19615

Table 3. Toluene Oxidation Activity Parameters Calculated after GCMS Analysis of Products at Different Time Intervals for Catalysts CH1 and CH2

activity	time (h)	catalyst dose (g)	toluene conc. (mL)	Cat/Tol ratio[g]	H_2O_2[a] conc.	C_T[b] (%)	S_{BAD}[c] (%)	Y_{BAD}[d] (%)	S_{BAL}[e] (%)	Y_{BAL}[f] (%)
Blank-1	18	0.0	2.0		0	0	0	0	0	0
Blank-2	18	0.0	2.0		3 equiv	4.57	38.57	2.85	37.43	1.71
				Catalyst **CH1**						
Act-1a	0.17	0.1	2.0	0.020	3 equiv	0	0	0	0	0
Act-1b	1	0.1	2.0	0.020	3 equiv	3.45	40.67	1.40	61.33	2.12
Act-1c	4	0.1	2.0	0.020	3 equiv	8.12	50.39	4.09	50.89	4.13
Act-1d	8	0.1	2.0	0.020	3 equiv	14.80	59.02	8.73	39.97	5.91
Act-1e	12	0.1	2.0	0.020	3 equiv	18.87	64.23	12.11	32.79	6.18
Act-1f	18	0.1	2.0	0.020	3 equiv	26.02	73.66	19.16	26.48	6.89
				Catalyst **CH2**						
Act-21	0.17	0.1	2.0	0.020	3 equiv	0	0	0	0	0
Act-2b	1	0.1	2.0	0.020	3 equiv	1.67	19.23	0.32	33.12	0.55
Act-2c	4	0.1	2.0	0.020	3 equiv	3.89	28.19	1.10	24.56	0.96
Act-2d	8	0.1	2.0	0.020	3 equiv	5.34	39.12	2.09	18.87	1.08
Act-2e	12	0.1	2.0	0.020	3 equiv	8.11	43.67	3.54	14.43	1.17
Act-2f	18	0.1	2.0	0.020	3 equiv	15.23	51.65	7.87	9.24	1.41

[a]H_2O_2 = 3 equiv to toluene. [b]C_T = conversion of toluene. [c]S_{BAL} = selectivity toward benzaldehyde. [d]Y_{BAL} = yield of benzaldehyde. [e]S_{BAL} = selectivity of benzyl alcohol. [f]Y_{BAL} = yield of benzyl alcohol. [g]Ratio calculated by the number of moles of the catalyst used (Cat)/number of moles of toluene (Tol) used for concerned activity.

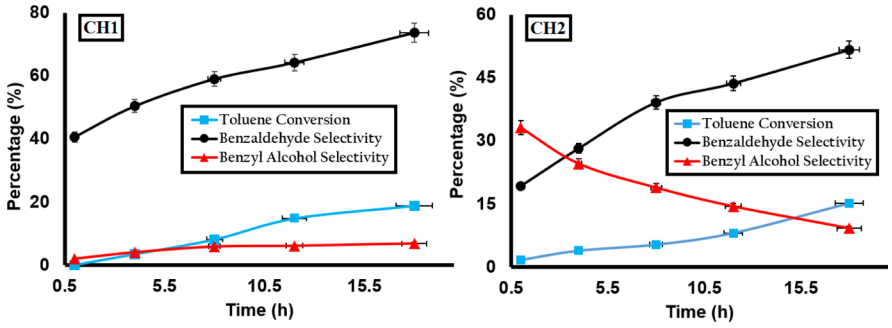

Figure 5. Catalytic performance of **CH1** and **CH2** for toluene oxidation at different time intervals (1, 4, 8, 12, and 18 h).

Table 4. Toluene Oxidation Activity Parameters Calculated after GCMS Analysis of Products for the Catalyst Dose Study

activity	time (h)	catalyst dose (g)	toluene conc. (mL)	Cat/Tol ratio	H_2O_2[a] conc.	C_T[b] (%)	S_{BAD}[c] (%)	Y_{BAD}[d] (%)	S_{BAL}[e] (%)	Y_{BAL}[f] (%)
Blank-1	18	0.0	2.0		0	0	0	0	0	0
Blank-2	18	0.0	2.0		3 equiv	4.57	38.57	2.85	37.43	1.71
Act-3a	18	0.02	2.0	0.0048	3 equiv	34.33	50.75	17.42	49.24	16.90
Act-3b	18	0.04	2.0	0.0096	3 equiv	34.59	50.84	17.58	49.15	17.01
Act-3c	18	0.06	2.0	0.0149	3 equiv	34.13	64.11	21.88	35.88	12.24
Act-3d	18	0.08	2.0	0.0048	3 equiv	29.08	60.04	17.46	23.74	6.90
Act-1f	18	0.1	2.0	0.0200	3 equiv	26.02	73.66	19.16	26.48	6.89

[a]H_2O_2 = 3 equiv to toluene. [b]C_T = conversion of toluene. [c]S_{BAL} = selectivity toward benzaldehyde. [d]Y_{BAL} = yield of benzaldehyde. [e]S_{BAL} = selectivity of benzyl alcohol. [f]Y_{BAL} = yield of benzyl alcohol.

$$\% \text{ Yield of products} = \frac{\% \text{ toluene conversion} \times \% \text{ product selectivity}}{100} \quad (6)$$

Blank 1 (carried out without an oxidant and catalyst) has shown no toluene conversion, whereas **Blank 2** has shown a 4.57% conversion of toluene (carried out in the presence of an oxidant only) after 18 h of oxidation activity.

2.2.1. Effect of Time. Extent of toluene oxidation with increasing time interval was evaluated for both of the catalysts **CH1** (**Act-1a** to **Act-1e**) and **CH2** (**Act-2a** to **Act-2e**) while keeping the catalyst dose (0.1 g) and concentration of toluene (2 mL) constant (Table 3). For checking out the extent of toluene oxidation at each time interval (i.e., 15 min and 1, 4, 8, 12, and 14 h), the sample aliquot was taken and analyzed. Products obtained after each activity were analyzed by GCMS, and the calculated parameters are enlisted in Table 3. No toluene conversion was detected after 15 min of toluene oxidation activity for **CH1** and **CH2**. With **CH1**, 3.45% C_T obtained after 1 h increased to 26.02% after 18 h of activity. 73.66% selectivity with 19.16% yield of benzaldehyde, whereas 26.48% selectivity with 6.89% yield for benzyl alcohol was obtained for catalyst **CH1** (Figure 5). With **CH2**, 1.67% C_T obtained after 1 h increased to 15.23% after 18 h of activity. 51.65% selectivity with 7.876% yield of benzaldehyde, whereas

https://doi.org/10.1021/acsomega.1c02163
ACS Omega 2021, 6, 19606−19615

9.24% selectivity with 1.41% yield for benzyl alcohol was obtained for catalyst **CH2** (Figure 5). Catalyst **CH1** was found to be more active for toluene oxidation giving more percent toluene conversion and further activities were carried out using **CH1**. The maximum catalytic efficiency of **CH1** to oxidize toluene oxidation attributed to their larger specific surface areas calculated from BET analysis (Table 2).

2.2.2. Effect of Catalyst Dose. For oxidation of toluene, the catalyst dose was varied in activities as 0.02 g (**Act-3a**), 0.04 g (**Act-3b**), 0.06 g (**Act-3c**), 0.08 g (**Act-3d**), and 0.1 g (**Act-1f**), while keeping the activity time (18 h) and concentration of toluene (2 mL) constant. Activity products were analyzed by GCMS, and benzaldehyde and benzyl alcohol were obtained as major products. Parameters such as percent conversion of toluene (C_T), product selectivity ($S_{product}$), and yield of specific products ($Y_{product}$) were calculated for each activity and are enlisted in Table 4. The maximum toluene conversion, that is, 34.59%, was attained using 0.04 g of catalyst dose giving 50.84% selectivity and 17.58% yield of benzaldehyde, whereas 49.15% selectivity and 17.01% yield were obtained for benzyl alcohol (Figure 6). 73.66% selectivity toward benzaldehyde

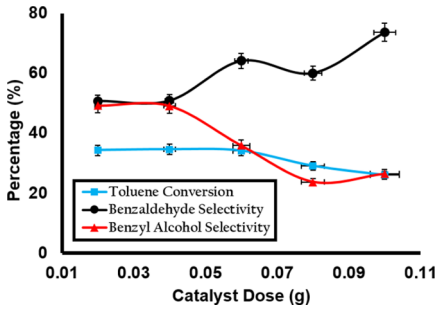

Figure 6. Catalytic performance of **CH1** for toluene oxidation using different catalyst doses (0.02, 0.04, 0.06, 0.08, and 1 g).

obtained with increasing catalyst dose up to 0.1 g is attributed to the more number of active sites being available for the oxidation process. Hence, due to the balanced ratio of substrate and active site, probability of attachment of toluene molecules to the active site of catalysts increased, giving benzaldehyde as an oxidation product more selectively.

2.2.3. Effect of Toluene Concentration. The effect of different toluene concentrations was evaluated using 2.2 mL (**Act-4a**), 2.0 mL (**Act-3c**), 1.8 mL (**Act-4b**), 1.6 mL (**Act-4c**), 1.4 mL (**Act-4d**), and 1.2 mL (**Act-4e**) of toluene, while keeping the time (18 h) and catalyst dose (0.06 g) constant. Toluene oxidation products after each activity were analyzed by GCMS and the calculated parameters are enlisted in Table 5. 40.62% toluene conversion was obtained using 1.6 mL of toluene during oxidation activity giving 56.97% selectivity and 26.79% yield of benzaldehyde, whereas 34.02% selectivity and 13.82% yield were obtained for benzyl alcohol (Figure 7).

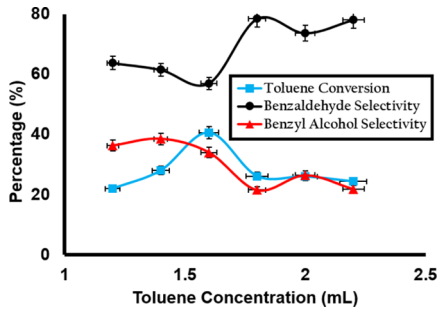

Figure 7. Catalytic performance of **CH1** for toluene oxidation using different toluene concentrations (1.2, 1.4, 1.6, 1.8, 2.0, and 2.2 mL).

78.42% selectivity with 20.51% yield of benzaldehyde were obtained during oxidation activity with 1.8 mL of concentration of toluene, and this selectivity is attributed to competition between active sites and toluene molecules getting on the catalyst surface and efficient conversion of it into benzaldehyde. Selectivity toward benzaldehyde was noticed to be greater for all the activities which are ascribed mainly to the adsorption competition between toluene and benzyl alcohol (oxidized product of toluene). As benzyl alcohol already occupied the active site of the catalyst, its oxidation to benzaldehyde is more favorable than adsorbing another molecule of toluene for oxidation. Further increase in toluene concentration up to 2.2 mL does not significantly alter the selectivity but conversion reduced due to increased collision in molecules and hence poorer yields were observed.

2.3. Catalyst Reusability. After the first cycle of toluene oxidation activity by **CH1**, oxidation products were centrifuged to separate the catalyst. The catalyst **CH1** was then washed with deionized water and DMSO, dried, and used again for up to six cycles. The percent toluene conversion and selectivity of benzyl alcohol and benzaldehyde by the **CH1** catalyst after successive catalytic cycles are shown in Figure 8. The 40.62, 28.03, 26.16, 26.02, 24.37, and 21.98% toluene conversions were obtained from catalytic activity cycle 1−6, respectively (Table 6). Efficient toluene conversion obtained after these

Table 5. Toluene Oxidation Activity Parameters Calculated after GCMS Analysis of Products for Different Toluene Concentrations

activity	time (h)	catalyst dose (g)	toluene conc. (mL)	Cat/Tol ratio	H_2O_2 conc[a]	C_T[b] (%)	S_{BAD}[c] (%)	Y_{BAD}[d] (%)	S_{BAL}[e] (%)	Y_{BAL}[f] (%)
Blank-1	18	0.0	2.0		0	0	0	0	0	0
Blank-2	18	0.0	2.0		3 equiv	4.57	38.57	2.85	37.43	1.71
Act-3c	18	0.06	2.0	0.0149	3 equiv	26.02	73.66	19.16	26.48	6.89
Act-4a	18	0.06	2.2	0.0135	3 equiv	24.37	78.07	19.02	21.92	5.34
Act-4b	18	0.06	1.8	0.0165	3 equiv	26.16	78.42	20.51	21.57	5.64
Act-4c	18	0.06	1.6	0.0186	3 equiv	40.62	56.97	26.79	34.02	13.82
Act-4d	18	0.06	1.4	0.0213	3 equiv	28.03	61.47	17.23	38.52	10.79
Act-4e	18	0.06	1.2	0.0248	3 equiv	21.98	63.71	14.00	36.28	7.97

[a]H_2O_2 = 3 equiv to toluene. [b]C_T = conversion of toluene. [c]S_{BAL} = selectivity toward benzaldehyde. [d]Y_{BAL} = yield of benzaldehyde. [e]S_{BAL} = selectivity of benzyl alcohol. [f]Y_{BAL} = yield of benzyl alcohol.

https://doi.org/10.1021/acsomega.1c02163
ACS Omega 2021, 6, 19606−19615

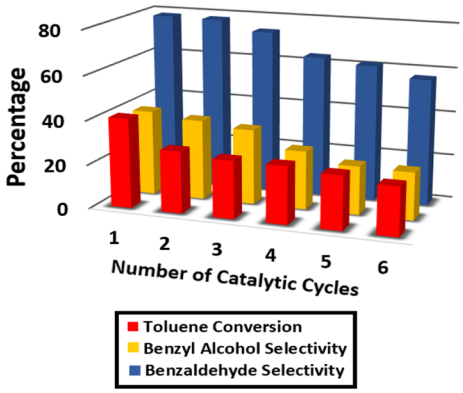

Figure 8. Percentages of toluene conversion and benzyl alcohol and benzaldehyde Selectivity by **CH1** after successive catalytic cycles.

catalytic activity cycles exhibited the potential of catalyst's reusability.

Table 6. % Toluene Conversion and Turnover Frequencies (TOFs) of Different Activity Cycles

cycles of catalytic activity	toluene conversion (%)	turn over frequency TOF (s−1)
1	40.62	1.94
2	28.03	1.43
3	26.16	1.39
4	26.02	1.32
5	24.37	1.11
6	21.98	1.01

The turnover frequency (TOF) of the different cycles is measured from the slope of the time versus conversion graphs of individual cycles.[31] The percent toluene conversion and turnover frequencies obtained after 18 h of catalytic activity cycles are enlisted in Table 6 and TOF trends are depicted in Figure 9. The TOFs calculated for successive activity cycles

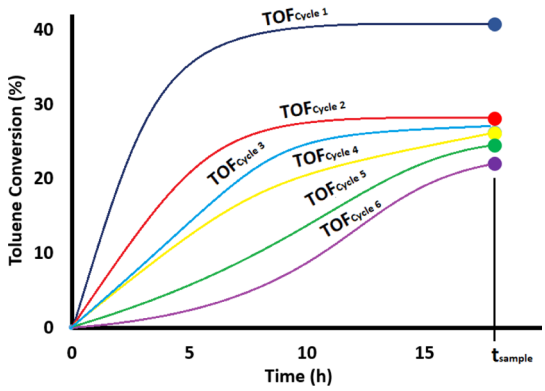

Figure 9. Turnover frequency (TOF) trends of each cycle by catalyst **CH1** after 18 h (t_{sample}) of catalytic activity.

were 1.94, 1.43, 1.39, 1.32, 1.11, and 1.01 s^{-1}, respectively. Values are in good agreement concerning each catalytic cycle, that is, not a major change in TOFs was observed which is a good indication of catalyst reusability.

FTIR spectra of catalyst **CH1** after recovery were recorded (Figure 10) giving no significant change in the peak position. The increase in transmittance observed is due to changing

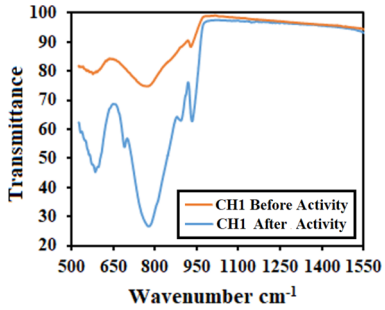

Figure 10. FTIR spectra of catalyst **CH1** before and after toluene oxidation activity.

texture of grains from crystalline-like appearance which is converted into a more powder form after cycles of activity.

2.4. Reaction Mechanism. Metal oxides are best-known as active species for C−H activation.[32] The reaction mechanism for the oxidation of toluene is attributed to the production of free radicals via C−H activation and a proposed mechanism is depicted in Figure 11.[33] The benzyl radical is formed by the homolytic cleavage of the C−H bond, and as a result, the benzyl radical ($Ph-CH_2^{\bullet}$) formed is adsorbed on the surface of the catalyst.[34] The hydroxyl radical ($OH^{\bullet}$) from hydrogen peroxide reacts with the benzyl radical to form benzyl alcohol which is further oxidized into benzaldehyde by the excess of hydroxyl radicals.[35] The oxidation process during these activities was reached to the conversion of toluene into benzaldehyde, and no benzoic acid was detected which may be due to the acidic nature of the catalyst.

3. CONCLUSIONS

To conclude the whole discussion, $MnMoO_4$ nanomaterials **CH1** and **CH2** have been synthesized from cheaper, facile, environmentally friendly, less-toxic, and abundant earth metal precursors. Synthesized nanomaterials were characterized using PXRD, SEM/EDX, UV−vis, PL, and BET techniques and their catalytic efficiencies were evaluated by direct oxidation of toluene into benzaldehyde selectively in the presence of H_2O_2 as an oxidant at 80 °C via C−H activation. The reaction parameters such as catalyst dose, time, and toluene concentration were varied to obtain the optimal conditions for the oxidation process. The high conversion rate of toluene, that is, 40.62%, was obtained after 18 h of oxidation activity with 0.06 g of catalyst CH1. More than 40% selectivity for benzaldehyde was attained for all the oxidation activities giving a maximum of 78% with 0.06 g of catalyst **CH1** after 18 h of activity. Catalyst durability was checked out using them for several cycles. Several catalytic cycles were run with **CH1** to evaluate catalyst reusability. Potential % toluene conversion was obtained for up to six cycles and their turnover frequencies were found to be 1.94−1.01 s^{-1}. FTIR spectra of catalyst **CH1** before and after recovery indicate no significant change. Important industrial products benzyl alcohol and benzaldehyde have been produced with notable yields and enhanced selectivities. The liquid-phase oxidation of toluene inhibits the use of hazardous chlorinated chemicals and byproducts as well. Moreover, the high conversion rate of toluene is primarily eccentric which proves the robustness and high potential of these catalysts under a milder, greener, and hazardous chlorine-free environment.

https://doi.org/10.1021/acsomega.1c02163
ACS Omega 2021, 6, 19606−19615

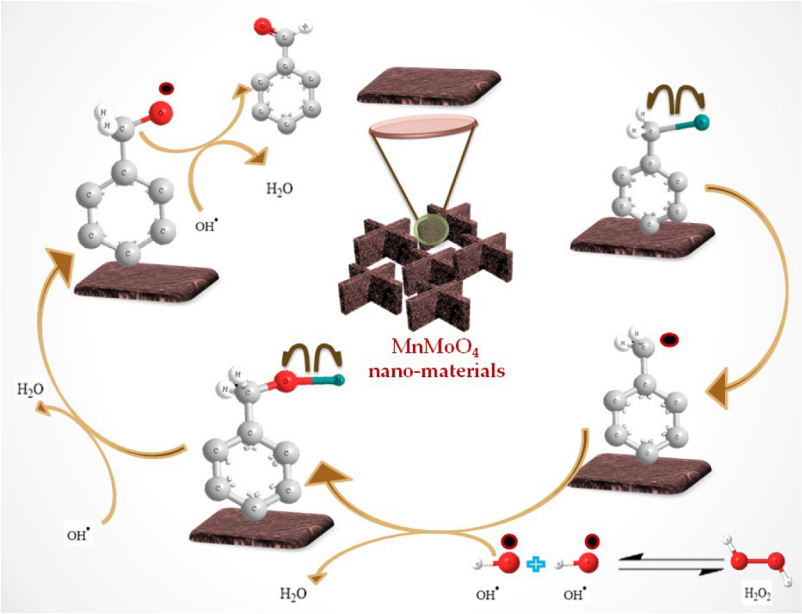

Figure 11. Reaction mechanism of the toluene oxidation over $MnMoO_4$.

4. EXPERIMENTAL SECTION

4.1. Chemicals. Manganese acetate $Mn(CH_3COO)_2$, molybdenum-VI oxide MoO_3, NaOH, isopropanol, dimethylsulfoxide (DMSO), toluene (purity greater than 99%), acetonitrile (HPLC grade), and hydrogen peroxide H_2O_2 (35% in water) were used. All the chemicals were of analytical grade, purchased from Merck, and used without further purification.

4.2. Synthesis. Materials **CH1** and **CH2** were synthesized via a simple solvothermal method. The **CH1** was synthesized by taking 30 mL of 0.5 M manganese acetate (3.5 g) solution in a flask and subjecting to stirring. Then, 30 mL of isopropanol was added to the reaction mixture which resulted in the formation of layers. To break down the layers, 10 mL of DMSO (acted as emulsifier) was added dropwise to the solution. The 0.5 M solution of MoO_3 (2.2 g) was prepared in NaOH separately and this alkaline solution was added dropwise to the abovementioned reaction mixture. The reaction was carried out for 1 h until white precipitates were formed. This mixture was transformed into a Teflon-lined autoclave container and kept in an oven for 18 h at 150 °C. After that, precipitates were filtered and washed several times with deionized water and DMSO to remove inorganic and organic impurities, respectively. Precipitates were air-dried first and then kept in an oven at 60 °C for 1 h. The yellowish-brown-colored crystalline material was obtained, characterized, and utilized for catalytic studies. The **CH2** was synthesized by the same method as used for **CH1** by taking 0.4 M solution of MoO_3 (1.73 g). A notable change has been noticed in the texture, color, and appearance of the synthesized materials by changing the ratio of MoO_3 during synthesis.

4.3. Characterization. PXRD measurements were performed via an X-ray diffractometer (Bruker, AXS D8) with Cu-Kα radiation (1.5406 Å) with a continuous scan of 6°/min in the 2θ range from 10 to 80°. Morphological features of catalysts were characterized by SEM (JEOL, JSM-6360 EO), and elemental composition was estimated through an EDX diffractometer (JEOL JSM-6360 LV). Optical characterization was performed using a UV spectrophotometer (Shimadzu) in the frequency range of 250−800 nm and a PL spectrophotometer at an excitation wavelength of 480 nm. The surface area and pore structure parameters were calculated by a Brunauer−Emmett−Teller (BET) analysis performed through Quantachrome Nova 2200e (Tokyo, Japan). The FTIR studies were performed for all samples with a Fourier transform infrared spectrometer in the range of wavenumber 500−4000 cm^{-1}. Toluene oxidation products were analyzed through gas chromatography and mass spectrometry (GCMS) (Shimadzu QP2010, MS Detector SPD 20A, Solvent: Acetonitrile, Column: C-18 (250 × 4.6 mm), Temperature; 80 °C).

4.4. Catalytic Oxidation of Toluene Activity. For catalytic oxidation of toluene activity, 0.1 g of catalysts **CH1** and **CH2** were dispersed in 8 mL of acetonitrile in a round-bottom flask and 2 mL of toluene was added into it. Then, 2.34 mL of 35% H_2O_2 (3 equiv to toluene) was added dropwise in half an hour to prevent immediate degradation of the oxidant. The reaction mixture was maintained at 80 °C and refluxed for 18 h. After that, the reaction mixture was cooled to room temperature and centrifuged to separate the catalysts. Oxidation of toluene was carried out for all the catalysts, and liquid products were analyzed through GCMS. Catalysts were washed, dried, and utilized for several cycles. FTIR spectra of the catalyst before and after catalytic activity testing were recorded.

Blank-1 activity for oxidation of toluene was performed without incorporating the catalyst and oxidant, whereas **Blank-2** activity was performed in the presence of an oxidant only. Different factors affecting the oxidation of toluene such as time, catalyst dose, and concentration of toluene were studied following the abovedescribed method.

To monitor the toluene oxidation at different time intervals, sample aliquots were taken out from the reaction mixture, that is, 15 min and 1, 4, 8, 12, and 18 h, keeping the catalyst dose (0.1 g) and concentration of toluene (2 mL) constant. Toluene oxidation at different time intervals was evaluated for both catalysts **CH1** (**Act-1a** to **Act-1e**) and **CH2** (**Act-2a** to **Act-2e**) and toluene conversion was obtained the maximum with the **CH1** catalyst. Based on the results of the previous activity,

https://doi.org/10.1021/acsomega.1c02163
ACS Omega 2021, 6, 19606−19615

a catalyst dose study was carried using **CH1**. The amount of catalyst **CH1** was varied as 0.02 g (**Act-3a**), 0.04 g (**Act-3b**), 0.06 g (**Act-3c**), 0.08 g (**Act-3d**), and 0.1 g (**Act-1f**) keeping the activity time (18 h) and concentration of toluene (2 mL) constant. The effect of different toluene concentrations was evaluated using 2.2 mL (**Act-4a**), 2.0 mL (**Act-3c**), 1.8 mL (**Act-4b**), 1.6 mL (**Act-4c**), 1.4 mL (**Act-4d**), and 1.2 mL (**Act-4e**) keeping the time (18 h) and catalyst dose (0.06 g) constant. Activity products were studied through GCMS, and percent toluene conversion, product yields, and selectivity were calculated.

■ AUTHOR INFORMATION

Corresponding Author

Ataf Ali Altaf − *Department of Chemistry, University of Okara, Okara 56300, Pakistan; Catalysis and Energy Research Center, University of Okara, Okara 56300, Pakistan;* orcid.org/0000-0001-8018-5890; Phone: +92-332-5049532; Email: atafali_altaf@yahoo.com

Authors

Hamza Shoukat − *Department of Chemistry, University of Gujrat, Gujrat 50700, Pakistan*

Muhammad Hamayun − *Department of Chemistry, University of Gujrat, Gujrat 50700, Pakistan*

Shaheed Ullah − *Department of Chemistry, University of Okara, Okara 56300, Pakistan*

Samia Kausar − *Department of Chemistry, University of Gujrat, Gujrat 50700, Pakistan*

Muhammad Hamza − *Department of Chemistry, University of Gujrat, Gujrat 50700, Pakistan*

Shabbir Muhammad − *Department of Physics, College of Science, King Khalid University, Abha 61413, Saudi Arabia*

Amin Badshah − *Department of Chemistry, Quaid-i-Azam University, Islamabad 45320, Pakistan*

Nasir Rasool − *Department of Chemistry, Government College University, Faisalabad 38000, Pakistan*

Muhammad Imran − *Department of Chemistry, Faculty of Science, King Khalid University, Abha 61413, Saudi Arabia*

Complete contact information is available at: https://pubs.acs.org/10.1021/acsomega.1c02163

Notes

The authors declare no competing financial interest.

■ ACKNOWLEDGMENTS

This research was mainly financially supported by Higher Education Commission Islamabad, Pakistan, under HEC-NRPU project no. 6492. S.M. from King Khalid University, Saudi Arabia, extend his appreciation to Deanship of Scientific Research at King Khalid University for funding the work through research project (R.G.P.2/128/42).

■ REFERENCES

(1) Wu, W.; Zhang, G.; Zhang, J.; Wang, G.; Tung, C.-H.; Wang, Y. Aerobic oxidation of toluene and benzyl alcohol to benzaldehyde using a visible light-responsive titanium-oxide cluster. *Chem. Eng. J.* **2021**, *404*, 126433.

(2) Kholkina, E.; Mäki-Arvela, P.; Lozachmeuer, C.; Barakov, R.; Shcherban, N.; Murzin, D. Y. Prins cyclisation of (-)-isopulegol with benzaldehyde over ZSM-5 based micro-mesoporous catalysts for production of pharmaceuticals. *Chin. J. Catal.* **2019**, *40*, 1713−1720.

(3) Loch, C.; Reusch, H.; Ruge, I.; Godelmann, R.; Pflaum, T.; Kuballa, T.; Schumacher, S.; Lachenmeier, D. W. Benzaldehyde in cherry flavour as a precursor of benzene formation in beverages. *Food Chem.* **2016**, *206*, 74−77.

(4) Satrio, J. A.; Doraiswamy, L. Production of benzaldehyde: a case study in a possible industrial application of phase-transfer catalysis. *Chem. Eng. J.* **2001**, *82*, 43−56.

(5) Malek, A. M.; Barchowsky, A.; Bowser, R.; Heiman-Patterson, T.; Lacomis, D.; Rana, S.; Ada Youk, A.; Talbott, E. O. Exposure to hazardous air pollutants and the risk of amyotrophic lateral sclerosis. *Environ. Pollut.* **2015**, *197*, 181−186.

(6) Kausar, S.; ul Ain, N.; Altaf, A. A.; Danish, M.; Basit, A.; Lal, B.; Muhammad, S.; Badshah, A.; Muhammad Kashif Javaid, H. Electrochemical and thermal catalytic studies of Co based molybdenum oxide nanomaterials for C H bond activation. *Inorg. Chim. Acta* **2021**, *517*, 120219.

(7) Lapari, S. S.; Parham, S. Oxidation of toluene and hydrogen peroxide catalyzed by Ni (II), Co (II), and Cu (II) Schiff base complexes. *Int. J. Eng. Sci. Invent* **2013**, *2*, 62−67.

(8) Parmeggiani, C.; Matassini, C.; Cardona, F. A step forward towards sustainable aerobic alcohol oxidation: new and revised catalysts based on transition metals on solid supports. *Green Chem.* **2017**, *19*, 2030−2050.

(9) (a) Wang, Y.; Arandiyan, H.; Scott, J.; Bagheri, A.; Dai, H.; Amal, R. Recent advances in ordered meso/macroporous metal oxides for heterogeneous catalysis: a review. *J. Mater. Chem. A* **2017**, *5*, 8825−8846. (b) Kausar, S.; Ali Altaf, A.; Hamayun, M.; Danish, M.; Zubair, M.; Naz, S.; Muhammad, S.; Zaheer, M.; Ullah, S.; Badshah, A. Soft template-based bismuth doped zinc oxide nanocomposites for photocatalytic depolymerization of lignin. *Inorg. Chim. Acta* **2020**, *502*, 119390. (c) Kausar, S.; Altaf, A. A.; Hamayun, M.; Rasool, N.; Hadait, M.; Akhtar, A.; Muhammad, S.; Badshah, A.; Shah, S. A. A.; Zakaria, Z. A. i-propylammonium lead chloride based perovskite photocatalysts for depolymerization of lignin under UV light. *Molecules* **2020**, *25*, 3520. (d) Altaf, A. A.; Ahmed, M.; Hamayun, M.; Kausar, S.; Waqar, M.; Badshah, A. Titania nano-fibers: a review on synthesis and utilities. *Inorg. Chim. Acta* **2020**, *501*, 119268. (e) Hamza, M.; Altaf, A. A.; Kausar, S.; Murtaza, S.; Rasool, N.; Gul, R.; Badshah, A.; Zaheer, M.; Ali Shah, S. A.; Zakaria, Z. A. Catalytic removal of alizarin red using chromium manganese oxide nanorods: Degradation and kinetic studies. *Catalysts* **2020**, *10*, 1150.

(10) Gallon, B. J.; Kojima, R. W.; Kaner, R. B.; Diaconescu, P. L. Palladium Nanoparticles Supported on Polyaniline Nanofibers as a Semi-Heterogeneous Catalyst in Water. *Angew. Chem., Int. Ed.* **2007**, *46*, 7251−7254.

(11) Anastas, P. *Warner JC Green Chemistry Theory and Practice*; Oxford University Press. G. B., 2000.

(12) Wen, C.; Yin, A.; Dai, W.-L. Recent advances in silver-based heterogeneous catalysts for green chemistry processes. *Appl. Catal., B* **2014**, *160−161*, 730−741.

(13) Chen, Q.; Zhang, X.; Su, S.; Xu, Z.; Li, N.; Li, Y.; Zhou, H.; Bao, M.; Yamamoto, Y.; Jin, T. Nanoporous Gold-Catalyzed Diboration of Methylenecyclopropanes via a Distal Bond Cleavage. *ACS Catal.* **2018**, *8*, 5901−5906.

(14) Li, F.; Guo, Y.; Wu, T.; Liu, Y.; Wang, W.; Gao, J. Platinum nano-catalysts deposited on reduced graphene oxides for alcohol oxidation. *Electrochim. Acta* **2013**, *111*, 614−620.

(15) Baig, R. B. N.; Nadagouda, M. N.; Varma, R. S. Ruthenium on chitosan: a recyclable heterogeneous catalyst for aqueous hydration of nitriles to amides. *Green Chem.* **2014**, *16*, 2122−2127.

(16) Ghosh, S.; Acharyya, S. S.; Tripathi, D.; Bal, R. Preparation of silver-tungsten nanostructure materials for selective oxidation of toluene to benzaldehyde with hydrogen peroxide. *J. Mater. Chem. A* **2014**, *2*, 15726−15733.

(17) Liu, H.; Yang, Q. Facile fabrication of nanoporous Au-Pd bimetallic foams with high catalytic activity for 2-nitrophenol reduction and SERS property. *J. Mater. Chem.* **2011**, *21*, 11961−11967.

(18) Adil, S.; Assal, M.; Kuniyil, M.; Khan, M.; Shaik, M. R.; Alwarthan, A.; Labis, J.; Siddiqui, M. R. Synthesis and comparative catalytic study of zinc oxide (ZnOx) nanoparticles promoted MnCO3, MnO2 and Mn2O3 for selective oxidation of benzylic alcohols using molecular oxygen. *Mater. Express* **2017**, *7*, 79−92.
(19) Wang, B.; Chi, C.; Xu, M.; Wang, C.; Meng, D. Plasma-catalytic removal of toluene over CeO 2 -MnO x catalysts in an atmosphere dielectric barrier discharge. *Chem. Eng. J.* **2017**, *322*, 679−692.
(20) Xu, J.; Sun, Y.; Lu, M.; Wang, L.; Zhang, J.; Qian, J.; Liu, X. Fabrication of hierarchical MnMoO4·H2O@MnO2 core-shell nanosheet arrays on nickel foam as an advanced electrode for asymmetric supercapacitors. *Chem. Eng. J.* **2018**, *334*, 1466−1476.
(21) Cao, Y.; Li, W.; Xu, K.; Zhang, Y.; Ji, T.; Zou, R.; Yang, J.; Qin, Z.; Hu, J. MnMoO4·4H2O nanoplates grown on a Ni foam substrate for excellent electrochemical properties. *J. Mater. Chem. A* **2014**, *2*, 20723−20728.
(22) Ghosh, D.; Giri, S.; Moniruzzaman, M.; Basu, T.; Mandal, M.; Das, C. K. α MnMoO4/graphene hybrid composite: high energy density supercapacitor electrode material. *Dalton Trans.* **2014**, *43*, 11067−11076.
(23) Mi, Y.; Huang, Z.; Zhou, Z.; Hu, F.; Meng, Q. Room-temperature synthesis of MnMoO4·H2O nanorods by the microemulsion-based method and its photocatalytic performance. *J. Phys.: Conf. Ser.* **2009**, *188*, 012056.
(24) Paul, A.; Dhar, S. S. Construction of hierarchical MnMoO4/NiFe2O4 nanocomposite: Highly efficient visible light driven photocatalyst in the degradation of different polluting dyes in aqueous medium. *Colloids Surf., A* **2020**, *585*, 124090.
(25) Holzwarth, U.; Gibson, N. The Scherrer equation versus the "Debye-Scherrer equation". *Nat. Nanotechnol.* **2011**, *6*, 534.
(26) Mittemeijer, E. J.; Welzel, U. The "state of the art" of the diffraction analysis of crystallite size and lattice strain. *J. Crystallogr.* **2008**, *223*, 552−560.
(27) Dini, G.; Ueji, R.; Najafizadeh, A.; Monir-Vaghefi, S. Flow stress analysis of TWIP steel via the XRD measurement of dislocation density. *Mater. Sci. Eng., A* **2010**, *527*, 2759−2763.
(28) Motevalizadeh, L.; Heidary, Z.; Abrishami, M. E. Facile template-free hydrothermal synthesis and microstrain measurement of ZnO nanorods. *Bull. Mater. Sci.* **2014**, *37*, 397−405.
(29) Feng, Y.; Lin, S.; Huang, S.; Shrestha, S.; Conibeer, G. Can Tauc plot extrapolation be used for direct-band-gap semiconductor nanocrystals? *J. Appl. Phys.* **2015**, *117*, 125701.
(30) Yi, D.; Hui, F.; Fengjun, Z.; Youchun, F.; Qicai, Z. Preparation of MnMoO4·XH2O (X=0.9, 1.5) by a Microemulsion Method under Different Manganese Precursors and Analysis of Their Band-gap Energy. *Rare Met. Mater. Eng.* **2017**, *46*, 68−72.
(31) De Vylder, A.; Lauwaert, J.; Van Auwenis, S.; De Clercq, J.; Thybaut, J. W. Catalyst Stability Assessment in a Lab-Scale Liquid-Solid (LS)2 Plug-Flow Reactor. *Catalysts* **2019**, *9*, 755.
(32) Li, X.; Lunkenbein, T.; Kröhnert, J.; Pfeifer, V.; Girgsdies, F.; Rosowski, F.; Schlögl, R.; Trunschke, A. Hydrothermal synthesis of bifunctional nanostructured manganese tungstate catalysts for selective oxidation. *Faraday Discuss.* **2016**, *188*, 99−113.
(33) (a) Mal, D. D.; Khilari, S.; Pradhan, D. Efficient and selective oxidation of toluene to benzaldehyde on manganese tungstate nanobars: a noble metal-free approach. *Green Chem.* **2018**, *20*, 2279−2289. (b) Pillai, U. R.; Sahle-Demessie, E. Vanadium phosphorus oxide as an efficient catalyst for hydrocarbon oxidations using hydrogen peroxide. *New J. Chem.* **2003**, *27*, 525−528.
(34) Baltaretu, C. O.; Lichtman, E. I.; Hadler, A. B.; Elrod, M. J. Primary atmospheric oxidation mechanism for toluene. *J. Phys. Chem. A* **2009**, *113*, 221−230.
(35) Rozanska, X.; Fortrie, R.; Sauer, J. Size-dependent catalytic activity of supported vanadium oxide species: oxidative dehydrogenation of propane. *J. Am. Chem. Soc.* **2014**, *136*, 7751−7761.

https://doi.org/10.1021/acsomega.1c02163
ACS Omega 2021, 6, 19606−19615